

RESEARCH ARTICLE | JUNE 15 2023

## Influence of random telegraph noise on quantum bit gate operation

Jackson Likens; Sanjay Prabhakar ; Ratan Lal; Roderick Melnik 



*Journal of Applied Physics* 133, 234301 (2023)

<https://doi.org/10.1063/5.0147810>



CrossMark

500 kHz or 8.5 GHz?  
And all the ranges in between.

Lock-in Amplifiers for your periodic signal measurements



Find out more



# Influence of random telegraph noise on quantum bit gate operation

Cite as: J. Appl. Phys. **133**, 234301 (2023); doi: [10.1063/5.0147810](https://doi.org/10.1063/5.0147810)

Submitted: 26 February 2023 · Accepted: 30 May 2023 ·

Published Online: 15 June 2023



Jackson Likens,<sup>1</sup> Sanjay Prabhakar,<sup>1,a)</sup>  Ratan Lal,<sup>2</sup> and Roderick Melnik<sup>3,4</sup> 

## AFFILIATIONS

<sup>1</sup>Department of Natural Science, D L Hubbard Center for Innovation, Loess Hill Research Center, Northwest Missouri State University, 800 University Drive, Maryville, Missouri 64468, USA

<sup>2</sup>Department of Computer Science, Northwest Missouri State University, 800 University Drive, Maryville, Missouri 64468, USA

<sup>3</sup>MS2Discovery Interdisciplinary Research Institute, M3AI Lab, Wilfrid Laurier University, 75 University Avenue, Waterloo, Ontario N3L 3V6, Canada

<sup>4</sup>BCAM, Bizkaia Technology Park, 48160 Derio, Spain

<sup>a)</sup>Author to whom correspondence should be addressed: [sanjay@nwmissouri.edu](mailto:sanjay@nwmissouri.edu)

## ABSTRACT

We consider the problem of analyzing spin-flip qubit gate operation in the presence of Random Telegraph Noise (RTN). Our compressive approach is the following. By using the Feynman disentangling operators method, we calculate the spin-flip probability of qubit driven by different kinds of composite pulses, e.g., Constant pulse (C-pulse), Quantum Well pulse (QW-pulse), and Barrier Potential pulse (BP-pulse) in the presence of RTN. When composite pulses and RTN act in the x-direction and z-direction respectively, we calculate the optimal time to achieve perfect spin-flip probability of qubit. We report that the highest fidelity of spin-flip qubit can be achieved by using C-pulse, followed by BP-pulse and QW-pulse. For a more general case, we have tested several pulse sequences for achieving high fidelity quantum gates, where we use the pulses acting in different directions. From the calculations, we find that high fidelity of qubit gate operation in the presence of RTN is achieved when QW-pulse, BP-pulse, and C-pulse act in the x-direction, y-direction, and z-direction, respectively. We extend our investigations for multiple QW and BP pulses while choosing the C-pulse amplitude constant in the presence of RTN. The results of calculation show that 98.5% fidelity can be achieved throughout the course of RTN that may be beneficial for quantum error correction.

08 August 2023 02:13:27

Published under an exclusive license by AIP Publishing. <https://doi.org/10.1063/5.0147810>

## I. INTRODUCTION

Qubits can be manipulated in a desired fashion by excellent architectural design in several physical devices, such as quantum dots, cavity quantum electrodynamics, superconducting devices, and Majorana fermions.<sup>1–18</sup> Manipulation of qubits in these devices seems promising in that one can make quantum logic gates and memory devices for various quantum information processing applications. Such devices require sufficiently short gate operation time combined with long coherent time.<sup>19–22</sup>

When a qubit is operated on by a classical bit, then its decay time is given by a relaxation time that is also supposed to be longer than the minimum time required to execute one quantum gate operation. International Technology Roadmap for Semiconductors (ITRS) suggests that the node length and gate oxide thickness in

CMOS technology for qubit gate operation is approaching approximately 1 nm. Hence, a leakage current from the source to drain through the channel as well as the gate to the channel through the gate oxide layer is unavoidable.<sup>23–27</sup> Recent experimental studies confirm that the oscillations of the drain current at both low and room temperatures may consider a source of Random Telegraph Noise (RTN) and most likely reduce the performance of qubit gate operations.<sup>23–27</sup>

In most cases, compared to coherent time, the dephasing time of qubits in the presence of noise is reduced by several orders of magnitude due to the coupling of qubits to the environment. The reduction of dephasing time depends on the specific dynamical coupling sequence where the principle of quantum mechanics is inevitably lost. Therefore, one might need to decouple the qubits from the environment and may consider a more robust topological

method to preserve a quantum state, enabling robust quantum memory.<sup>6,29,30</sup> Hence, to make quantum computers, one needs to find an efficient and experimentally feasible algorithm that overcomes the issues of undesired interactions of qubits with RTN or the environment because these interactions destroy the quantum coherence and generate errors and loss of fidelity.<sup>31–33</sup> In quantum computing language, this phenomenon is called decoherence. For example, experimental observations reported that in GaAs quantum dots, decoherence time  $T_2^* \approx 10$  ns and coherent time  $T_1 \approx 0.1$  ms, whereas for Si,  $T_2^* \approx 100$  ns and  $T_1 \approx 0.1$  ms.<sup>34–46</sup> There are several possible ways to overcome the issues of decoherence, as, for example, through fidelity recovery by applying error-correcting codes, decoherence free subspace coding, noiseless subsystem coding, dynamical decoupling from hot bath, numerical design of pulse sequence, which is more robust to experimental inhomogeneities, and optimal control pulses.<sup>47–61</sup>

In this paper, we design several control pulses acting on a single bit-flip computational basis states in the presence of Random Telegraph Noise (RTN).<sup>62–66</sup> The choice of modeling parameters for RTN is the same as that of experimentally observed RTN in Ref. 23. For example, choosing a small noise correlation time in RTN provides very fast jumps, whereas a large noise correlation time provides slow jumps. Hence, checking performance of qubit under RTN in this paper resembles the realistic form of RTN that was recently discussed in experimental studies in Ref. 23. The present work identifies different regimes of operating parameters in the designed control pulses that eliminate the series of phase and dynamical errors and increase the recovery of high fidelities of spin-flip qubit gate operation. The designed composite pulses, named as Constant pulse (C-pulse), Quantum Well pulse (QW-pulse) and Barrier Potential pulse (BP-pulse), act on a qubit in the presence of Random Telegraph Noise (RTN). The amplitude of C-pulse is constant with time, whereas three composite pulse sequences of different time widths form QW-pulse and BP-pulse. For multiple QW and BP pulses, we have chosen six composite pulse sequences. The calculations of spin-flip qubit gate operation under RTN at various noise correlation times as well as various energy amplitudes of noise strength provide an indication of the most efficient ways to perform algorithms for achieving high fidelity quantum gates for quantum circuits and quantum error correction. In what follows, we report that when the qubits are driven by pulses in the x-direction and the RTN act in the z-direction; then, the C-pulse induces less systematic errors compared to BP-pulse followed by QW-pulse. For a more general case, we have tested all the possible combinations of the pulses acting in arbitrary x-, y-, and z-directions in the presence of RTN and show that the maximum fidelity of qubit gate operation can be achieved if QW-pulse acts in the x-direction, BP-pulse acts in the y-direction, and C-pulse acts in the z-direction. For multiple QW and BP pulse sequences, 99% fidelity can be achieved throughout the course of RTN. This useful information may be utilized to identify experimentally feasible pulses in the presence of RTN for the design of next generation quantum circuits.

The rest of the paper is organized as follows. In Sec. II, we provide a theoretical description of finding exact unitary operator using the Feynman disentangling operator scheme of the model Hamiltonian of a qubit driven by several control pulses in the

presence of RTN. In Sec. III, we analyze two main results: (i) fidelity of qubits driven by a pulse in the x-direction and by the RTN in the z-direction and (ii) the fidelity of qubits driven by individual C-pulse and single and multiple forms of QW and BP pulses that act in the x-, y-, and z-directions in the presence of the RTN still acting in the z-direction. Finally, we conclude the results in Sec. IV.

## II. MODEL HAMILTONIAN

The Hamiltonian of a single qubit is written as<sup>67</sup>

$$H(t) = \sum_{i \in \{x,y,z\}} \frac{1}{2} [a_i(t) + \eta_i(t)] \cdot \sigma_i, \quad (1)$$

where  $a_i(t)$  is the energy amplitude of the external control pulse,  $\eta_i(t)$  is the energy amplitude of the random telegraph noise, and  $\sigma_i$  are the Pauli spin matrices. Our goal is to design several composite pulses that provide high probability of spin-flip qubit in the presence of RTN. Hence, we model the mathematical function of pulses as

$$a_C(t) = \frac{\cos(t/t_0)}{|\cos(t/t_0)|}, \quad (2)$$

where  $t_0 = 8$  ps for C-pulse. For BP and QW composite pulses, we model the function as

$$a_{BP/QW}(t) = \frac{\sin(t/t_0 + r_0)}{|\sin(t/t_0 + r_0)|}, \quad (3)$$

where  $t_0 = 1.8$  ps and  $r_0 = -0.6$  for BP-pulse and  $t_0 = 2.0$  ps and  $r_0 = 2.56$  for QW-pulse. The designed C-pulse, BP-pulse, and QW-pulse obtained from Eqs. (2) and (3) are shown in Fig. 1. Notice that the amplitude of C-pulse is constant whereas the combination of three composite pulses that form QW-pulse is shown in Fig. 1(b) and the combination of three composite pulses that form BP-pulse sequence is shown in Fig. 1(c). In the Hamiltonian (1), the RTN only acts in the z-direction because random RTN jumps originated mostly due to leakage current from gate oxide to the channel as spins are transported from source to drain, as demonstrated experimentally in Ref. 23. The energy amplitude of the RTN changes randomly between  $-\Delta$  and  $\Delta$ , where  $\Delta$  is the maximum energy amplitude. Hence, we model the RTN trajectory as

$$\Xi(t, t_i) = \sum_{i=1}^N \Theta(t - t_i), \quad (4)$$

$$\eta_z(t) = (-1)^{\Xi(t,t_i)} \Delta, \quad (5)$$

where  $\Theta(t - t_i)$  is a Heaviside step function and the random jumps time,  $t_i$  is expressed as

$$t_i = \sum_{j=1}^N -\tau_c \ln(p_j), \quad (6)$$

08 August 2023 02:13:27

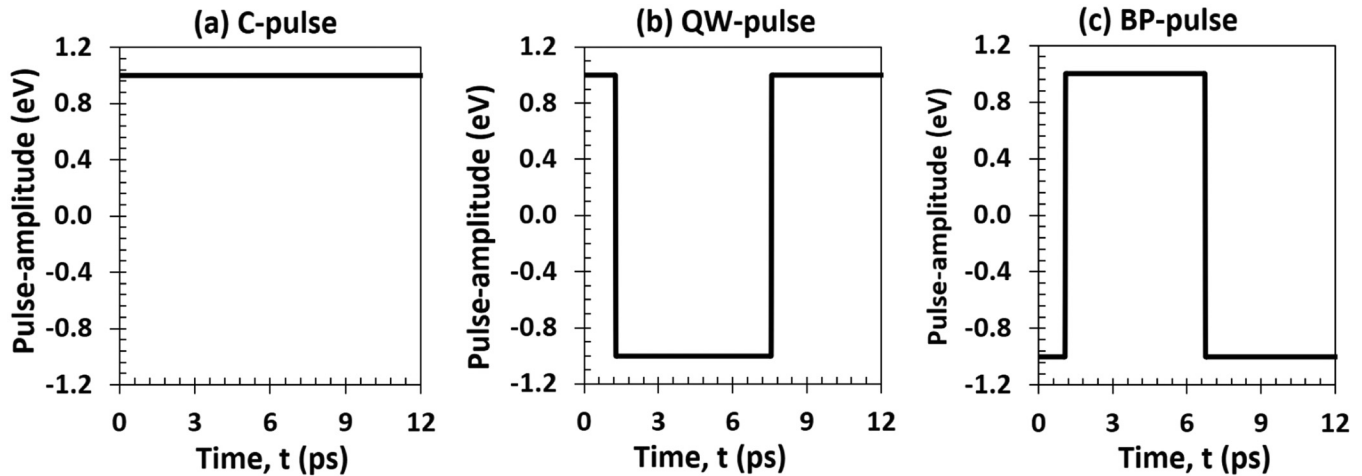


**FIG. 1.** The designed pulses for (a) C-pulse, (b) QW-pulse, and (c) BP-pulse that operate on qubits to achieve high fidelity quantum gates under random telegraph noise. The functional form of these pulses is shown in Eqs. (2) and (3). We chose  $t_0 = 8$  ps for C-pulse,  $t_0 = 1.8$  ps and  $r_0 = -0.6$  for BP-pulse, and  $t_0 = 2.0$  ps and  $r_0 = 2$  for QW-pulse.

where  $\tau$  is the RTN correlation time and  $p_j \in (0, 1)$  is the random numbers. Two RTN functions are shown in Figs. 2 and 3. In this paper, we have kept the duration of RTN trajectories same for all the pulses. For the realistic simulations of spin-flip qubit, we have chosen 600 randomly generated RTN functions (see Fig. 6). As can be seen in Fig. 2, there is large density of RTN jumps in the vicinity

of small correlation times,  $\tau_c = 1$  ps. On the other hand, as  $\tau_c$  increases, the density of RTN jumps decreases that can be seen in Fig. 3. Note that the modeling parameters of RTN trajectories shown in Figs. 2 and 3 are in close agreement with the experimental trajectories of RTN reported in Ref. 23. To find the system dynamics, an average value over different RTN sample trajectories

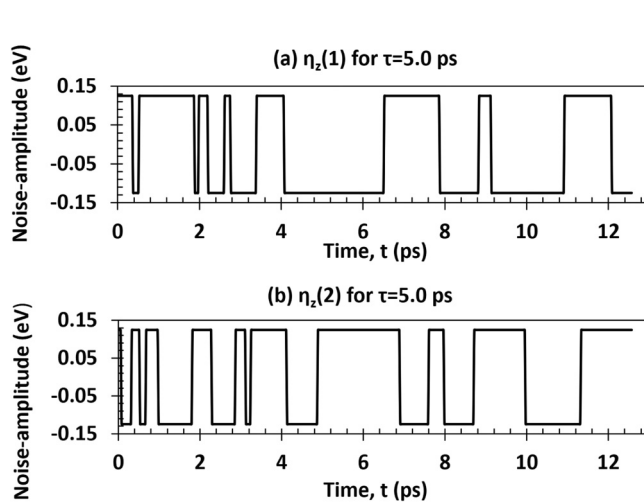


**FIG. 2.** Simulations of random telegraph noise (RTN) as a function of time are obtained from Eq. (4). Here, we chose the correlation time  $\tau_c = 5.0$  ps and  $\Delta = 0.125$  eV. Note that the density of RTN jumps between  $\pm \Delta$  is random that is shown in (a) and (b). Here, only two RTN functions are shown for demonstration purpose but in realistic simulations of finding high fidelity of spin-flip quantum gates, 300 RTN trajectories have been chosen.

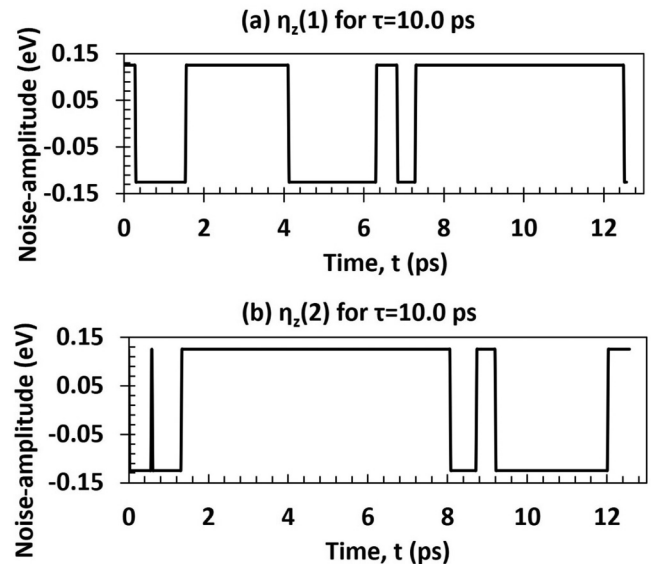


**FIG. 3.** Same as to Fig. 2 but  $\tau_c = 20.0$  ps. Notice that the jumps in RTN are significantly decreased as correlation time  $\tau_c$  increases from 5.0 ps in Fig. 2 to 20.0 ps in Fig. 3. For large  $\tau_c$ , there are almost no jumps in the RTN function.

08 August 2023 02:13:27

is chosen to find the density matrix,

$$\rho(t) = \lim_{N \rightarrow \infty} \frac{1}{N} \sum_{k=1}^N U_k(t) \rho_0 U_k^\dagger(t), \quad (7)$$

where  $\rho_0$  is the initial state of the system and  $\{U_k\}$  is the unitary time evolution of the qubit under the influence of control pulses (see Fig. 1) and RTN (see Figs. 2 and 3). We write the unitary time evolution operator as

$$U_k(t) = T e^{-i/\hbar \int_0^t dt H(t)}, \quad (8)$$

where  $T$  is the time ordering parameter. We apply the Feynman disentangling operator scheme and find the evolution operator as follows. The Hamiltonian  $H(t)$  in (1) or (8) can be written as

$$H(t) = H_+ s_+ + H_- s_- + H_z s_z, \quad (9)$$

where

$$H_+ = \frac{1}{2} (a_x(t) - i a_y(t)), \quad (10)$$

$$H_- = \frac{1}{2} (a_x(t) + i a_y(t)), \quad (11)$$

$$H_z = a_z(t) + \eta_z(t), \quad (12)$$

and  $s_\pm = (\sigma_x \pm i \sigma_y)/2$  and  $s_z = \sigma_z/2$ . In the disentangled form, the unitary time evolution operator (8) can be written as

$$U_k(t) = \exp(\alpha(t) s_+) \exp(\beta(t) s_z) \exp(\gamma(t) s_-), \quad (13)$$

where  $\alpha(t)$ ,  $\beta(t)$ , and  $\gamma(t)$  are unknown that can be found by using the Feynman disentangling operator method.<sup>6,8,68,69</sup> We write  $H(t)$  of (9) as

$$H(t) = \xi s'_+ + (H_+ - \xi) s'_+ + H_z s'_z + H_- s'_-, \quad (14)$$

where

$$\alpha(t) = -\frac{i}{\hbar} \int_0^t \xi(t) dt. \quad (15)$$

In the disentangled form, let

$$s'_\mu(t) = \exp(-\alpha s_+) s_\mu \exp(\alpha s_+), \quad (16)$$

and differentiating Eq. (16) with respect to  $\alpha$ , we can write

$$\frac{ds'_\mu(t)}{d\alpha} = \exp(-\alpha s_+) [s_\mu, s_+] s_\mu \exp(\alpha s_+), \quad (17)$$

and utilizing initial condition,  $s'_\mu(0) = s_\mu$ , we find  $s'_+ = s_+$ ,  $s'_0 = s_0 + s_+ \alpha$ ,  $s'_- = s_- - s_+ \alpha^2 - 2s_0 \alpha$ . Substituting Eq. (14) in

Eq. (8), we can write the unitary time evolution operator as

$$U_k(t) = e^{\alpha(t) s_+} T e^{-i/\hbar \int_0^t h(\alpha) dt}, \quad (18)$$

where

$$h(\alpha) = (H_+ - \xi + H_z \alpha - H_- \alpha^2) s_+ + H_z s_z + H_- s_- - 2H_- s_z \alpha. \quad (19)$$

Equating coefficient of  $s_+$  to zero, we write

$$\frac{d\alpha}{dt} = -\frac{i}{\hbar} \left[ \frac{1}{2} (a_x - i a_y) + (a_z + \eta_z) \alpha - \frac{1}{2} (a_x + i a_y) \alpha^2 \right]. \quad (20)$$

Hence,  $s_+$  of (19) in (18) is completely disentangled and, thus, unitary time evolution operator (18) can be written in the disentangled form as

$$U_k(t) = e^{\alpha(t) s_+} T e^{-i/\hbar \int_0^t H'(s'_\mu, \alpha) dt}, \quad (21)$$

where

$$H'(s'_\mu, \alpha) = \xi s'_z + (H_z - 2H_- \alpha - \xi) s'_z + H_- s'_-. \quad (22)$$

Now, consider

$$\beta(t) = -\frac{i}{\hbar} \int_0^t \xi(t) dt, \quad (23)$$

$$s'_\mu(t) = \exp(-\beta s_z) s_\mu \exp(\beta s_z), \quad (24)$$

and differentiate Eq. (24) with respect to  $\beta$ , we can write

$$\frac{ds'_\mu(t)}{d\alpha} = \exp(-\alpha s_+) [s_\mu, s_z] s_\mu \exp(\alpha s_z). \quad (25)$$

Utilizing initial condition,  $s'_\mu(0) = s_\mu$ , we find  $s'_z = s_z$ ,  $s'_- = s_- \exp(\beta)$  and substituting Eq. (22) in Eq. (21), we can write the unitary time evolution operator as

$$U_k(t) = e^{\alpha(t) s_+} e^{\beta(t) s_z} T e^{-i/\hbar \int_0^t (H_0 - 2H_- \alpha - H_- \xi) s_z + H_- s_- dt}. \quad (26)$$

Equating coefficient of  $s_z$  to zero, we write

$$\frac{d\beta}{dt} = -\frac{i}{\hbar} [a_z + \eta_z - (a_x + i a_y)]. \quad (27)$$

Hence,  $s_z$  of (26) is completely disentangled and thus unitary time evolution operator (26) can be written in the disentangled form as

$$U_k(t) = e^{\alpha(t) s_+} e^{\beta(t) s_z} T e^{-i/\hbar \int_0^t H''(s'_\mu, \alpha, \beta) dt}, \quad (28)$$

where

$$H''(s'_\mu, \alpha, \beta) = \chi s'_- + (H_- e^\beta - \chi) s'_-, \quad (29)$$

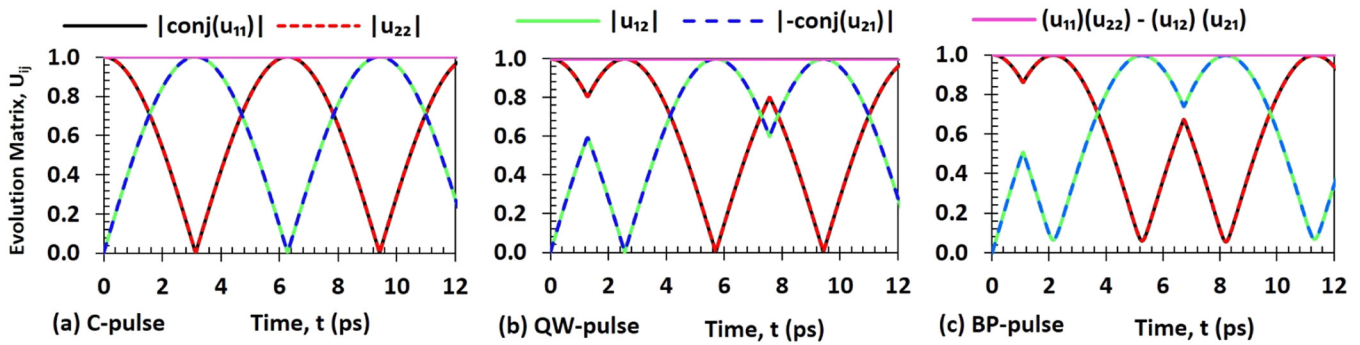


**FIG. 4.** Components of the evolution operator [see Eq. (35)] with respect to time for C-pulse in (a), QW-pulse in (b), and BP-pulse in (c). As can be seen in (a)–(c), we find that  $|u_{11}^*| = |u_{22}|$  and  $|u_{12}| = |-u_{21}^*|$  as well as  $(u_{11})(u_{22}) - (u_{12})(u_{21}) = 1$ . Hence, we confirmed that the components of the unitary time evolution operator obtained from the Feynman disentangling operator technique are in good agreement with the theoretical descriptions of the evolution matrix in quantum mechanics.

$$\gamma(t) = -\frac{i}{\hbar} \int_0^t \chi(t) dt, \quad (30)$$

$$s'_\mu(t) = \exp(-\gamma s_-) s_\mu \exp(\alpha s_-). \quad (31)$$

Differentiating Eq. (31) with respect to  $\gamma$ , we can write

$$\frac{ds'_\mu(t)}{d\gamma} = \exp(-\gamma s_-) [s_\mu, s_-] s_\mu \exp(\alpha s_-), \quad (32)$$

and utilizing initial condition,  $s'_\mu(0) = s_\mu$ , we find  $s'_- = s_-$ . Substituting Eq. (29) in Eq. (26), we can write the unitary time evolution operator as

$$U_k(t) = e^{\alpha(t)s_+} e^{\beta(t)s_z} e^{\gamma(t)s_-} T e^{-\frac{i}{\hbar} \int_0^t (H_- \exp(\beta) - \chi) s'_- dt}. \quad (33)$$

Equating coefficient of  $s_z$  to zero, we write

$$\frac{d\gamma}{dt} = -\frac{i}{\hbar} \left[ \frac{1}{2} (a_x + i a_y) \right]. \quad (34)$$

Hence, unitary time evolution operator (33) is completely disentangled. Finally, the exact unitary time evolution operator (33) can be written as

$$U_k(t) = \begin{pmatrix} \exp(\frac{\beta}{2}) + \alpha \gamma \exp\{-\frac{\beta}{2}\} & \alpha \exp(-\frac{\beta}{2}) \\ \gamma \exp(-\frac{\beta}{2}) & \exp(-\frac{\beta}{2}) \end{pmatrix}. \quad (35)$$

Since (35) is the exact time evolution operator in the disentangled form, we can construct the density matrix of (7) and find the fidelity of qubit as

$$\phi = \text{tr}\{\rho_f^\dagger \rho_T\}, \quad (36)$$

where  $\rho_f = U_f \rho_0 U_f^\dagger$  is the final state of the system and  $\rho_T$  is the final desired state of the qubit, where the pulse sequence ends. Here,  $U_f$  is a quantum gate that is independent of the initial state

preparation. Since all prepared state takes several channel routes on the Bloch sphere due to the presence of random telegraph noise, one may compute diamond norm and consider it as a specific metric to measure the distance between two quantum channels over all the samples of RTN.<sup>70</sup> The measurement of fidelity, that we find in this paper, is another popular metric to compute the distance between two quantum states.<sup>28</sup> In practice, it is often the case that we do not know the state of the particles (e.g., electrons emerging from linear accelerator lab or some probabilities of two different quantum entanglement states), i.e., the particles are in a mixed state and the density matrix for the states are not idempotent. However, in this paper, we chose  $U_f$  as a Pauli X-gate and prepared the idempotent pure initial state  $|0\rangle = (0, 0, 0, 1)_{2 \times 2}$  and final state  $|1\rangle = (1, 0, 0, 0)_{2 \times 2}$ . Then we found the spin-flip probability by using Eq. (36). The key tool for finding the system

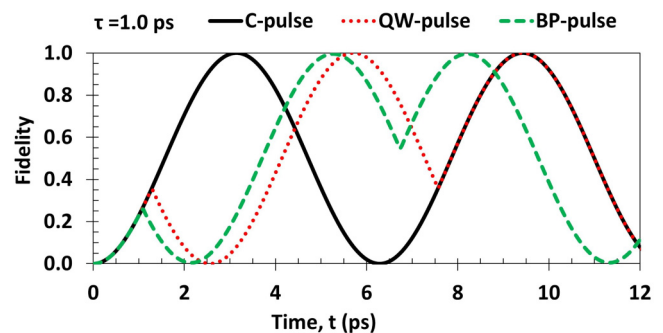


**FIG. 5.** Fidelity of spin-flip qubit, obtained from Eq. (36), as a function of RTN correlation time for C-pulse, QW-pulse and BP-pulse. Here, we chose  $\Delta = 0.125$  eV. As can be seen, tuning of perfect fidelity extends to a large RTN correlation time for C-pulse due to short optimal gate operation time ( $t = 3.14$  ps for C-pulse,  $t = 9.42$  ps for QW-pulse and  $t = 8.20$  ps for BP-pulse, see Fig. 5). At large RTN correlation time, where there are no jumps in RTN, BP-pulse can be used to recover the lost fidelities over the other two pulses (e.g., fidelity of BP-pulse is larger than C-pulse and QW-pulse at large RTN correlation time).



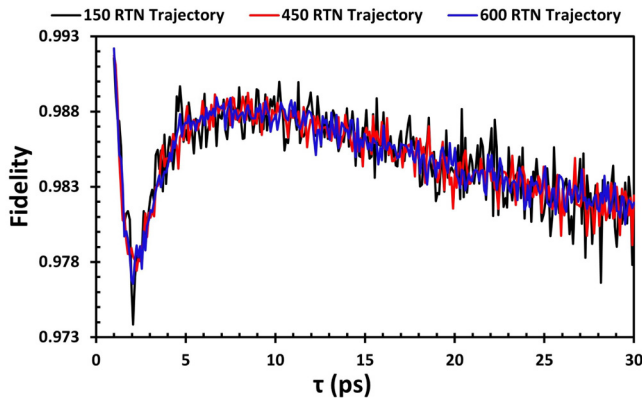


**FIG. 6.** Fidelity of spin-flip qubit as a function of RTN correlation time,  $\tau$ , for QW-pulse at 150 RTN trajectories (black line), 450 RTN trajectory (red line), and 600 RTN trajectory (green line). As can be seen, fluctuations in the fidelity decrease as we increase the number of RTN trajectories. In this paper, we use 600 RTN trajectories to investigate the influence of RTN on the fidelity of qubit for C-pulse, QW-pulse, and BP-pulse. We chose  $\Delta = 0.125$  eV.

dynamics of Eq. (8) is the use of the Feynman disentangling operator scheme.<sup>6,8,68,69</sup> We have chosen 600 RTN trajectories for the simulations and consider  $\hbar = a_{\max} = 1$ .

### III. RESULTS AND DISCUSSIONS

In Fig. 4, we have plotted the components of the evolution operator (35) of C-pulse in (a), QW-pulse in (b), and BP-pulse in (c) for RTN correlation time,  $\tau_C = 1.0$  ps. The data in these plots show that  $u_{22} = |\text{conj}(u_{11})|$  and  $u_{12} = |-\text{conj}(u_{21})|$  for C-pulse,

QW-pulse, and BP-pulse as well as  $|U_k(t, 0)| = 1$ . Hence, we confirmed that the evolution matrix obtained from the Feynman disentangling operator method is very accurate. In Fig. 5, we have plotted the fidelity of spin-flip qubit with respect to the evolution of time for C-pulse, QW-pulse, and BP-pulse. As can be seen, the perfect fidelity can be achieved at  $t = 3.14$  ps for C-pulse,  $t = 9.42$  ps for QW-pulse, and  $t = 8.20$  ps for BP-pulse. We consider these times as the optimum times for achieving high fidelity of spin-flip qubit in the presence of RTN. Notice that the optimum time for spin-flip qubit is the smallest for C-pulse (i.e.,  $t = 3.14$  ps) but the optimum time for BP-pulse is smaller (i.e.,  $t = 8.20$  ps) than in the case of the QW-pulse (i.e.,  $t = 9.42$  ps) because the C-pulse has constant energy amplitude whereas the width of the QW-pulse is larger than the width of BP-pulse (e.g., see Fig. 1). In other words, QW-pulse lasts longer than the BP-pulse during the spin-flip qubit gate operation. When noise correlation time is large ( $\tau_c > 2$ ), then decreasing RTN jumps increase the fluctuations in fidelity vs correlation time. In Fig. 6, as can be seen, an increase in the number of RTN trajectories reduces the fluctuations in finding the average value of fidelity. Hence in this paper we take 600 RTN trajectories to investigate the influence of RTN on the average value of fidelity of qubit gate operation.

We consider the C-pulse, QW-pulse, and BP-pulse acting in the x-direction and RTN in z-direction in the Hamiltonian (1) and plotted the fidelity of spin-flip qubit with respect to the RTN correlation time in Fig. 7. Note that Fig. 7(a) is reproduced results of Ref. 28, where we have chosen exactly the same pulse as well as same RTN. In other words, RTN vanishes at the optimal time. In Fig. 7(b), we have plotted the fidelity of qubit driven by C-pulse, QW-pulse and BP-pulse (see Fig. 1) in the presence of RTN (see Figs. 2 and 3). Note that in Fig. 7(b), we have kept same RTN for all the pulses that lasts much longer than the optimal time. As can

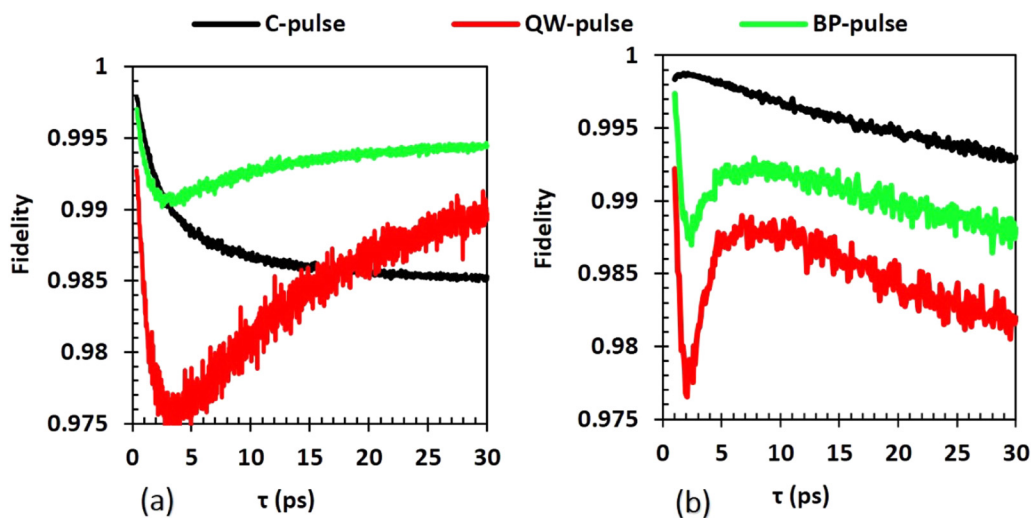


**FIG. 7.** Fidelity of spin-flip qubit as a function of RTN correlation time,  $\tau$ , for C-pulse, QW-pulse, and BP-pulse. Note that (a) is reproduced results of that of Ref. 28 by choosing the same control pulses and the same RTN trajectory, where the duration of RTN and the pulse sequence is the same. In (b), the fidelity is obtained by using the Feynman disentangling operator method, where the duration of RTN is kept same for all the pulses (see Figs. 2 and 3). We chose  $\Delta = 0.125$  eV.

08 August 2023 02:13:27

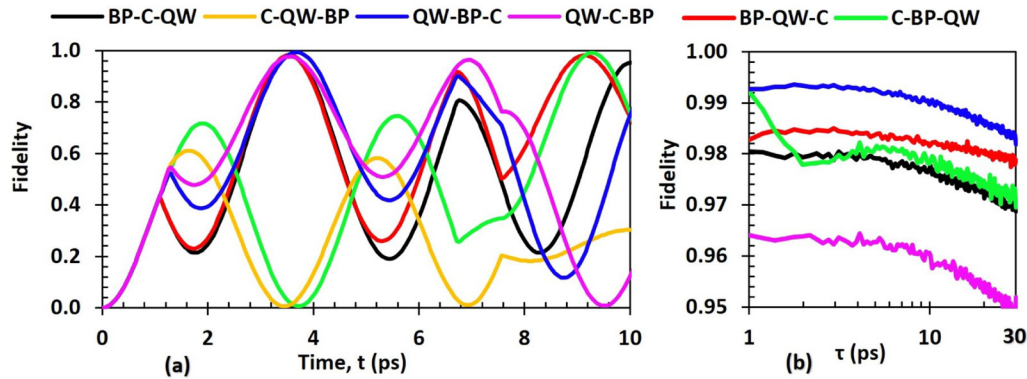


**FIG. 8.** (a) Fidelity of spin-flip qubit as a function of time for the pulse sequences shown in the systematic orders, e.g., for BP-C-QW pulse sequence, BP-pulse acts in the x-direction, C-pulse acts in the y-direction, and QW-pulse acts in the z-direction. As can be seen, the optimal time pulse for BP-C-QW is 3.57 ps, for BP-QW-C is 3.53 ps, for C-BP-QW is 9.46 ps, for QW-BP-C is 3.66 ps, and for QW-C-BP is 3.57 ps. For the C-QW-BP pulse, fidelity is very small and may not be useful for achieving high fidelity quantum gates. (b) Fidelity of spin-flip qubit as a function of RTN correlation time,  $\tau$  for  $\Delta = 0.125$  eV for several pulse sequences is shown. As can be seen, QW-BP-C pulse has better performance than all the other pulses for achieving high fidelity quantum gates with respect to RTN correlation time. Nevertheless, the fidelities for all the pulses shown in Fig. 7(b) are larger than 92%. Such a small error induced by RTN can be corrected for application in qubit gate operation.

be seen, in the regime of small RTN correlation time ( $\tau_c \approx 1.0$  ps), larger than 99% fidelity can be observed for all the three pulses, e.g., C-pulse, QW-pulse, and BP-pulse due to the fact that the single qubit does not have sufficiently large time to drift along the

direction of densely populated random telegraph noise (see Fig. 2). Note that the RTN function is dense in the vicinity of zero correlation time but has no jumps in the vicinity of infinite correlation time (e.g., the density of noise jumps decreases as  $\tau_c$  increases, see

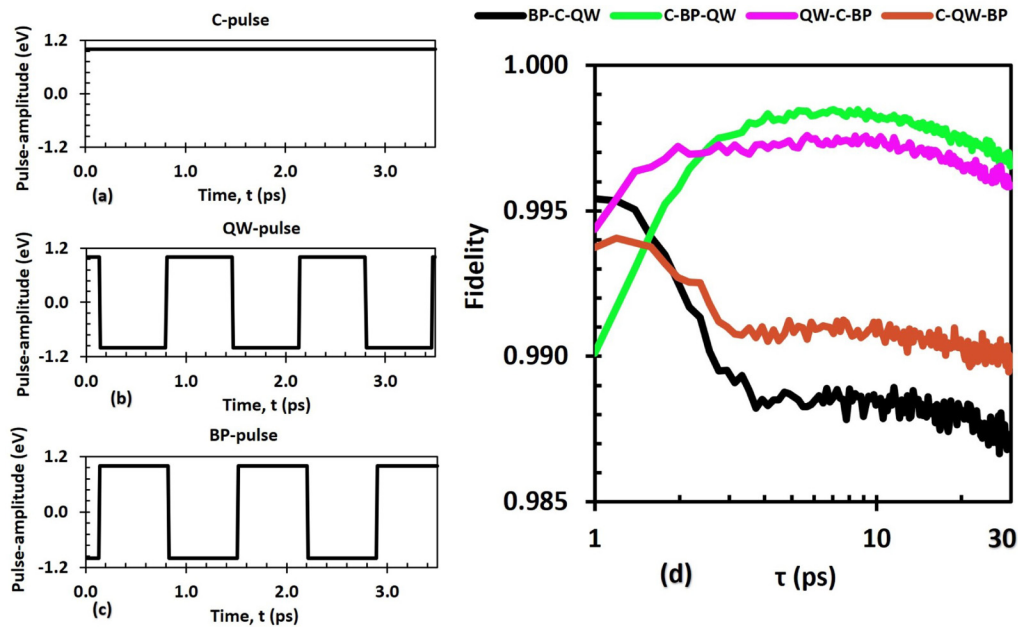


**FIG. 9.** Same as Fig. 8(b) but different forms of pulse sequence that has different optimal times to achieve a large fidelity. Nevertheless, the fidelities for all the pulses shown in Fig. 9 are larger than 98%. Such a small error induced by RTN can be corrected for application in the qubit gate operation. The optimal time for BP-C-QW pulse is 3.30 ps, for C-BP-QW is 3.43 ps, for QW-C-BP is 3.38 ps, and for C-QW-BP is 3.26 ps. Fidelities of QW-BP-C pulse and BP-QW-C pulse are less than 15%, which is not useful for quantum computing and error correction.



Figs. 2 and 3). In Fig. 7, we also observed minima at the noise correlation time,  $\tau \approx 3.0$  ps for BP-pulse and QW-pulse, due to the fact that as the jumps in RTN slowed down then qubit stays in the RTN state that let the qubit to drift along the noise direction. For large RTN correlation time, or there is less jumps in RTN, the qubit of BP-pulse and QW-pulse recovers most of its lost fidelity.

As shown in Fig. 8, for the pulses acting in all three directions and RTN in the z-direction, we can achieved high fidelity of spin-flip qubit only when QW-pulse acts in the x-direction, BP-pulse acts in the y-direction and C-pulse acts in the z-direction [blue plot in Fig. 8(b)]. The optimum time for such pulse sequences is  $t = 3.66$  ps that can be seen in the fidelity of spin-flip qubit-vs-time in Fig. 8(a). Note that we have tested all the other possible combinations of pulses as shown in Fig. 8(a) to achieve the optimal time for high fidelity of qubit. As can be seen in Fig. 8(b), the fidelities of spin-flip qubit for all the pulses are still above 95% and can still be used for quantum error correction and quantum information processing. In Fig. 9(a), we use multiple QW- and BP-pulse sequences and plotted the fidelity of several pulse sequences acting in all three directions in the presence of RTN. As can be seen in Fig. 9(b), the fidelity is larger than 98.5% and may be useful for quantum computing and quantum error correction codes.

#### IV. CONCLUSION

We have shown a possible way to achieve high fidelity of spin-flip qubit gate operation using several control pulses (e.g., C-pulse, QW-pulse, and BP-pulse) in the presence of random telegraph noises. In Fig. 7(b), we have shown that the C-pulse can be used for receiving high fidelity of spin-flip qubit gate operation due to its small optimal gate operation time. In Fig. 8, when the pulses acting in all three directions, we have tested several pulse sequences for achieving high fidelity quantum gates and reported that QW-pulse acting in the x-direction, BP-pulse acting in the y-direction and C-pulse acting in the z-direction can be used to provide high fidelity of qubit gate operation in the presence of RTN. Regardless of RTN conditions, the fidelities of spin-flip qubit gate operations for these pulses are larger than 95%. We can further improve to receive perfect fidelity by using multiple forms of QW- and BP-pulse sequences. In particular, in Fig. 9(b), we have shown systemic orders of pulse sequences and calculated the optimal time that can tune the fidelities larger than 98.5% throughout the course of RTN. Since the modeling parameters of RTN resemble the experimentally observed RTN in Ref. 23, one can use QW-pulse, BP-pulse, and C-pulse to transport the qubit for several different kinds of quantum gate operation that may have applications in the solid-state realization of quantum computing and quantum information processing.

#### ACKNOWLEDGMENTS

The simulations were performed at BARTIK High-Performance Cluster (National Science Foundation, Grant No. CNS-1624416, USA) in Northwest Missouri State University. J.L. and S.P. acknowledge the Northwest Missouri State University for providing financial support to present these results at American Physical Society March meeting in Chicago (2022). R.M. is acknowledging the support of NSERC Discovery and CRC Programs.

#### AUTHOR DECLARATIONS

##### Conflict of Interest

The authors have no conflicts to disclose.

##### Author Contributions

**Jackson Likens:** Conceptualization (supporting). **Sanjay Prabhakar:** Conceptualization (lead); Data curation (lead). **Ratan Lal:** Conceptualization (supporting). **Roderick Melnik:** Conceptualization (supporting).

#### DATA AVAILABILITY

The data that support the findings of this study are available from the corresponding author upon reasonable request.

#### REFERENCES

- <sup>1</sup>M.-S. Choi, C. Bruder, and D. Loss, "Spin-dependent Josephson current through double quantum dots and measurement of entangled electron states," *Phys. Rev. B* **62**, 13569 (2000).
- <sup>2</sup>G. Burkard, D. Loss, and D. P. DiVincenzo, "Coupled quantum dots as quantum gates," *Phys. Rev. B* **59**, 2070 (1999).
- <sup>3</sup>X. Hu and S. D. Sarma, "Hilbert-space structure of a solid-state quantum computer: Two-electron states of a double-quantum-dot artificial molecule," *Phys. Rev. A* **61**, 062301 (2000).
- <sup>4</sup>T. S. Koh, J. K. Gamble, M. Friesen, M. Eriksson, and S. Coppersmith, "Pulse-gated quantum-dot hybrid qubit," *Phys. Rev. Lett.* **109**, 250503 (2012).
- <sup>5</sup>D. Xiao, M.-C. Chang, and Q. Niu, "Berry phase effects on electronic properties," *Rev. Mod. Phys.* **82**, 1959 (2010).
- <sup>6</sup>S. Prabhakar, J. Raynolds, A. Inomata, and R. Melnik, "Manipulation of single electron spin in a GaAs quantum dot through the application of geometric phases: The Feynman disentangling technique," *Phys. Rev. B* **82**, 195306 (2010).
- <sup>7</sup>S. Prabhakar, R. Melnik, and L. L. Bonilla, "Gate control of berry phase in III-V semiconductor quantum dots," *Phys. Rev. B* **89**, 245310 (2014).
- <sup>8</sup>S. Prabhakar, R. Melnik, and A. Inomata, "Geometric spin manipulation in semiconductor quantum dots," *Appl. Phys. Lett.* **104**, 142411 (2014).
- <sup>9</sup>U. Vool, S. Shankar, S. Mundhada, N. Ofek, A. Narla, K. Sliwa, E. Zalusky-Geller, Y. Liu, L. Frunzio, R. Schoelkopf, and S. M. Girvin, "Continuous quantum non-demolition measurement of the transverse component of a qubit," *Phys. Rev. Lett.* **117**, 133601 (2016).
- <sup>10</sup>H.-K. Lau and M. B. Plenio, "Universal continuous-variable quantum computation without cooling," *Phys. Rev. A* **95**, 022303 (2017).
- <sup>11</sup>F. Yoshihara, T. Fuse, S. Ashhab, K. Kakuyanagi, S. Saito, and K. Semba, "Superconducting qubit-oscillator circuit beyond the ultrastrong-coupling regime," *Nat. Phys.* **13**, 44 (2017).
- <sup>12</sup>D. J. Clarke, J. D. Sau, and S. D. Sarma, "A practical phase gate for producing bell violations in Majorana wires," *Phys. Rev. X* **6**, 021005 (2016).
- <sup>13</sup>L. Grünhaupt, M. Spiecker, D. Gusenkova, N. Maleeva, S. T. Skacel, I. Takmakov, F. Valenti, P. Winkel, H. Rotzinger, W. Wernsdorfer, and A. V. Ustinov, "Granular aluminium as a superconducting material for high-impedance quantum circuits," *Nat. Mater.* **18**, 816 (2019).
- <sup>14</sup>Y. Zhong, H.-S. Chang, K. Satzinger, M.-H. Chou, A. Bienfait, C. Conner, É. Dumur, J. Grebel, G. Peairs, R. Povey, and D. I. Schuster, "Violating Bell's inequality with remotely connected superconducting qubits," *Nat. Phys.* **15**, 741 (2019).
- <sup>15</sup>P. Kurpiers, M. Pechal, B. Royer, P. Magnard, T. Walter, J. Heinsoo, Y. Salathé, A. Akin, S. Storz, J.-C. Besse, and S. Gasparinetti, "Quantum communication with time-bin encoded microwave photons," *Phys. Rev. Appl.* **12**, 044067 (2019).
- <sup>16</sup>Y. Xu, W. Cai, Y. Ma, X. Mu, L. Hu, T. Chen, H. Wang, Y. Song, Z.-Y. Xue, Z.-Q. Yin, and L. Sun, "Single-loop realization of arbitrary nonadiabatic

08 August 2023 02:13:27

holonomic single-qubit quantum gates in a superconducting circuit," *Phys. Rev. Lett.* **121**, 110501 (2018).

<sup>17</sup>X. Li, Y. Ma, J. Han, T. Chen, Y. Xu, W. Cai, H. Wang, Y. Song, Z.-Y. Xue, Z.-Q. Yin, and L. Sun, "Perfect quantum state transfer in a superconducting qubit chain with parametrically tunable couplings," *Phys. Rev. Appl.* **10**, 054009 (2018).

<sup>18</sup>C. Müller, J. H. Cole, and J. Lisenfeld, "Towards understanding two-level-systems in amorphous solids: Insights from quantum circuits," *Rep. Prog. Phys.* **82**, 124501 (2019).

<sup>19</sup>D. Loss and D. P. DiVincenzo, "Quantum computation with quantum dots," *Phys. Rev. A* **57**, 120 (1998).

<sup>20</sup>V. N. Golovach, A. Khaetskii, and D. Loss, "Phonon-induced decay of the electron spin in quantum dots," *Phys. Rev. Lett.* **93**, 016601 (2004).

<sup>21</sup>S. Amasha, K. MacLean, I. P. Radu, D. Zumbühl, M. Kastner, M. Hanson, and A. Gossard, "Electrical control of spin relaxation in a quantum dot," *Phys. Rev. Lett.* **100**, 046803 (2008).

<sup>22</sup>A. Balocchi, Q. Duong, P. Renucci, B. Liu, C. Fontaine, T. Amand, D. Lagarde, and X. Marie, "Full electrical control of the electron spin relaxation in GaAs quantum wells," *Phys. Rev. Lett.* **107**, 136604 (2011).

<sup>23</sup>Z. Li, M. Sotto, F. Liu, M. K. Husain, H. Yoshimoto, Y. Sasago, D. Hisamoto, I. Tomita, Y. Tsuchiya, and S. Saito, "Random telegraph noise from resonant tunnelling at low temperatures," *Sci. Rep.* **8**, 1 (2018).

<sup>24</sup>F. Liu, K. Ibukuro, M. K. Husain, Z. Li, J. Hillier, I. Tomita, Y. Tsuchiya, H. Rutt, and S. Saito, "Manipulation of random telegraph signals in a silicon nanowire transistor with a triple gate," *Nanotechnology* **29**, 475201 (2018).

<sup>25</sup>S. Singh, E. T. Mannila, D. S. Golubev, J. T. Peltonen, and J. P. Pekola, "Determining the parameters of a random telegraph signal by digital low pass filtering," *Appl. Phys. Lett.* **112**, 243101 (2018).

<sup>26</sup>X. Zhan, Y. Xi, Q. Wang, W. Zhang, Z. Ji, and J. Chen, "Dual-point technique for multi-trap RTN signal extraction," *IEEE Access* **8**, 88141 (2020).

<sup>27</sup>H. Yang, M. Robitaille, X. Chen, H. Elgabra, L. Wei, and N. Y. Kim, "Random telegraph noise of a 28-nm cryogenic MOSFET in the coulomb blockade regime," *IEEE Electron Device Lett.* **43**, 5 (2021).

<sup>28</sup>M. Möttönen, R. de Sousa, J. Zhang, and K. B. Whaley, "High-fidelity one-qubit operations under random telegraph noise," *Phys. Rev. A* **73**, 022332 (2006).

<sup>29</sup>J. Jing, L.-A. Wu, M. Byrd, J. Q. You, T. Yu, and Z.-M. Wang, "Nonperturbative leakage elimination operators and control of a three-level system," *Phys. Rev. Lett.* **114**, 190502 (2015).

<sup>30</sup>Ł. Cywiński, R. M. Lutchyn, C. P. Nave, and S. D. Sarma, "How to enhance dephasing time in superconducting qubits," *Phys. Rev. B* **77**, 174509 (2008).

<sup>31</sup>J. Simon, F. Calderon-Vargas, E. Barnes, and S. E. Economou, "Fast noise-resistant control of donor nuclear spin qubits in silicon," *Phys. Rev. B* **101**, 205307 (2020).

<sup>32</sup>J. Truong and X. Hu, "Decoherence of coupled flip-flop qubits due to charge noise," [arXiv:2104.07485](https://arxiv.org/abs/2104.07485) (2021).

<sup>33</sup>E. Ferraro, D. Rei, M. Paris, and M. De Michielis, "Universal set of quantum gates for the flip-flop qubit in the presence of 1/f noise," *EPJ Quantum Technol.* **9**, 1 (2022).

<sup>34</sup>H. Bluhm, S. Foletti, I. Neder, M. Rudner, D. Mahalu, V. Umansky, and A. Yacoby, "Dephasing time of GaAs electron-spin qubits coupled to a nuclear bath exceeding 200  $\mu$ s," *Nat. Phys.* **7**, 109 (2011).

<sup>35</sup>J. R. Petta, A. C. Johnson, J. M. Taylor, E. A. Laird, A. Yacoby, M. D. Lukin, C. M. Marcus, M. P. Hanson, and A. C. Gossard, "Coherent manipulation of coupled electron spins in semiconductor quantum dots," *Science* **309**, 2180 (2005).

<sup>36</sup>B. M. Maune, M. G. Borselli, B. Huang, T. D. Ladd, P. W. Deelman, K. S. Holabird, A. A. Kiselev, I. Alvarado-Rodriguez, R. S. Ross, A. E. Schmitz, and M. Sokolich, "Coherent singlet-triplet oscillations in a silicon-based double quantum dot," *Nature* **481**, 344 (2012).

<sup>37</sup>J. Pla, K. Y. Tan, J. P. Dehollain, W. H. Lim, J. J. Morton, D. N. Jamieson, A. S. Dzurak, and A. Morello, "A single-atom electron spin qubit in silicon," *Nature* **489**, 541 (2012).

<sup>38</sup>F. K. Malinowski, F. Martins, T. B. Smith, S. D. Bartlett, A. C. Doherty, P. D. Nissen, S. Fallahi, G. C. Gardner, M. J. Manfra, C. M. Marcus, and F. Kuemmeth, "Spin of a multielectron quantum dot and its interaction with a neighboring electron," *Phys. Rev. X* **8**, 011045 (2018).

<sup>39</sup>M. Friesen, J. Ghosh, M. Eriksson, and S. Coppersmith, "A decoherence-free subspace in a charge quadrupole qubit," *Nat. Commun.* **8**, 15923 (2017).

<sup>40</sup>F. Martins, F. K. Malinowski, P. D. Nissen, S. Fallahi, G. C. Gardner, M. J. Manfra, C. M. Marcus, and F. Kuemmeth, "Negative spin exchange in a multielectron quantum dot," *Phys. Rev. Lett.* **119**, 227701 (2017).

<sup>41</sup>Y. He, S. Gorman, D. Keith, L. Kranz, J. Keizer, and M. Simmons, "A two-qubit gate between phosphorus donor electrons in silicon," *Nature* **571**, 371 (2019).

<sup>42</sup>J. Geng, Y. Wu, X. Wang, K. Xu, F. Shi, Y. Xie, X. Rong, and J. Du, "Experimental time-optimal universal control of spin qubits in solids," *Phys. Rev. Lett.* **117**, 170501 (2016).

<sup>43</sup>B.-J. Liu, X.-K. Song, Z.-Y. Xue, X. Wang, and M.-H. Yung, "Plug-and-play approach to nonadiabatic geometric quantum gates," *Phys. Rev. Lett.* **123**, 100501 (2019).

<sup>44</sup>R. E. Throckmorton, E. Barnes, and S. D. Sarma, "Environmental noise effects on entanglement fidelity of exchange-coupled semiconductor spin qubits," *Phys. Rev. B* **95**, 085405 (2017).

<sup>45</sup>X.-C. Yang, M.-H. Yung, and X. Wang, "Neural-network-designed pulse sequences for robust control of singlet-triplet qubits," *Phys. Rev. A* **97**, 042324 (2018).

<sup>46</sup>C.-H. Huang and H.-S. Goan, "Robust quantum gates for stochastic time-varying noise," *Phys. Rev. A* **95**, 062325 (2017).

<sup>47</sup>N. Ofek, A. Petrenko, R. Heeres, P. Reinhold, Z. Leghtas, B. Vlastakis, Y. Liu, L. Frunzio, S. Girvin, L. Jiang, and M. Mirrahimi, "Extending the lifetime of a quantum bit with error correction in superconducting circuits," *Nature* **536**, 441 (2016).

<sup>48</sup>M. H. Michael, M. Silveri, R. Brierley, V. V. Albert, J. Salmilehto, L. Jiang, and S. M. Girvin, "New class of quantum error-correcting codes for a bosonic mode," *Phys. Rev. X* **6**, 031006 (2016).

<sup>49</sup>B. J. Brown, D. Loss, J. K. Pachos, C. N. Self, and J. R. Wootton, "Quantum memories at finite temperature," *Rev. Mod. Phys.* **88**, 045005 (2016).

<sup>50</sup>A. Reiserer, N. Kalb, M. S. Blok, K. J. van Bemmelen, T. H. Taminiau, R. Hanson, D. J. Twitchen, and M. Markham, "Robust quantum-network memory using decoherence-protected subspaces of nuclear spins," *Phys. Rev. X* **6**, 021040 (2016).

<sup>51</sup>H.-K. Lau and M. B. Plenio, "Universal quantum computing with arbitrary continuous-variable encoding," *Phys. Rev. Lett.* **117**, 100501 (2016).

<sup>52</sup>B.-H. Liu, X.-M. Hu, J.-S. Chen, C. Zhang, Y.-F. Huang, C.-F. Li, G.-C. Guo, G. B. U. Karpas, F. F. Fanchini, J. Piilo, and S. Maniscalco, "Time-invariant entanglement and sudden death of nonlocality," *Phys. Rev. A* **94**, 062107 (2016).

<sup>53</sup>A. Castro, J. Werschnik, and E. K. Gross, "Controlling the dynamics of many-electron systems from first principles: A combination of optimal control and time-dependent density-functional theory," *Phys. Rev. Lett.* **109**, 153603 (2012).

<sup>54</sup>X. Wang, L. S. Bishop, J. Kestner, E. Barnes, K. Sun, and S. D. Sarma, "Composite pulses for robust universal control of singlet-triplet qubits," *Nat. Commun.* **3**, 997 (2012).

<sup>55</sup>M. Jenei, E. Potanina, R. Zhao, K. Y. Tan, A. Rossi, T. Tanttu, K. W. Chan, V. Sevriuk, M. Möttönen, and A. Dzurak, "Waiting time distributions in a two-level fluctuator coupled to a superconducting charge detector," *Phys. Rev. Res.* **1**, 033163 (2019).

<sup>56</sup>S. L. Rudge and D. S. Kosov, "Fluctuating-time and full counting statistics for quantum transport in a system with internal telegraphic noise," *Phys. Rev. B* **100**, 235430 (2019).

<sup>57</sup>F. Motzoi, E. Halperin, X. Wang, K. B. Whaley, and S. Schirmer, "Backaction-driven, robust, steady-state long-distance qubit entanglement over lossy channels," *Phys. Rev. A* **94**, 032313 (2016).

<sup>58</sup>C. Dickel, J. J. Wesdorp, N. K. Langford, S. Peiter, R. Sagastizabal, A. Bruno, B. Criger, F. Motzoi, and L. DiCarlo, "Chip-to-chip entanglement of transmon qubits using engineered measurement fields," *Phys. Rev. B* **97**, 064508 (2018).

- <sup>59</sup>P. Kurpiers, P. Magnard, T. Walter, B. Royer, M. Pechal, J. Heinsoo, Y. Salathé, A. Akin, S. Storz, S. Besse, J.-C. Gasparinetti, A. Blais, and A. Wallraff, "Deterministic quantum state transfer and remote entanglement using microwave photons," *Nature* **558**, 264 (2018).
- <sup>60</sup>P. Campagne-Ibarcq, E. Zalts-Geller, A. Narla, S. Shankar, P. Reinhold, L. Burkhardt, C. Axline, W. Pfaff, L. Frunzio, R. Schoelkopf, and M. H. Devoret, "Deterministic remote entanglement of superconducting circuits through microwave two-photon transitions," *Phys. Rev. Lett.* **120**, 200501 (2018).
- <sup>61</sup>G. Dridi, M. Mejatty, S. J. Glaser, and D. Sugny, "Robust control of a not gate by composite pulses," *Phys. Rev. A* **101**, 012321 (2020).
- <sup>62</sup>E. Paladino, Y. Galperin, G. Falci, and B. Altshuler, "1/f noise: Implications for solid-state quantum information," *Rev. Mod. Phys.* **86**, 361 (2014).
- <sup>63</sup>J. Bergli and L. Faoro, "Exact solution for the dynamical decoupling of a qubit with telegraph noise," *Phys. Rev. B* **75**, 054515 (2007).
- <sup>64</sup>Y. M. Galperin, B. Altshuler, J. Bergli, and D. Shantsev, "Non-Gaussian low-frequency noise as a source of qubit decoherence," *Phys. Rev. Lett.* **96**, 097009 (2006).
- <sup>65</sup>L. Faoro and L. Viola, "Dynamical suppression of 1/f noise processes in qubit systems," *Phys. Rev. Lett.* **92**, 117905 (2004).
- <sup>66</sup>G. Falci, A. D'Arrigo, A. Mastellone, and E. Paladino, "Dynamical suppression of telegraph and 1/f noise due to quantum bistable fluctuators," *Phys. Rev. A* **70**, 040101 (2004).
- <sup>67</sup>M. A. Nielsen and I. L. Chuang, *Quantum Computation and Quantum Information* (Cambridge University Press, Cambridge, 2000).
- <sup>68</sup>R. P. Feynman, "An operator calculus having applications in quantum electrodynamics," *Phys. Rev.* **84**, 108 (1951).
- <sup>69</sup>V. S. Popov, "Feynman disentangling of noncommuting operators and group representation theory," *Phys.-Usp.* **50**, 1217 (2007).
- <sup>70</sup>G. Benenti and G. Strini, "Computing the distance between quantum channels: Usefulness of the fano representation," *J. Phys. B* **43**, 215508 (2010).